In Situ Oxidation of Reduced Graphene Oxide Membranes by Peracetic Acid for Dye Desalination

Erda Deng[1], Kai Chen[1], Aubrey E. Quigley[2], Mengqi Yuan[1], Lingxiang Zhu[3, 4], Zachary T. Kralles[5], Benny D. Freeman[2], Ning Dai*[5], and Haiqing Lin*[1]

[1] Department of Chemical and Biological Engineering, University at Buffalo, The State University of New York, Buffalo, NY 14260, USA

[2] John J. McKetta Jr. Department of Chemical Engineering, University of Texas at Austin, Austin, TX, 78712, USA

[3] U.S. Department of Energy, National Energy Technology Laboratory, Pittsburgh, PA, 15236, USA

[4] NETL Support Contractor, 626 Cochran Mill Road, Pittsburgh, PA 15236, USA

[5] Department of Civil, Structural and Environmental Engineering, University at Buffalo, The State University of New York, Buffalo, NY 14260, USA

[*] Corresponding authors. Tel: 716-645-4015, Email: ningdai@buffalo.edu (N. Dai); Tel: +1-716-645-1856, Email: haiqingl@buffalo.edu (H. Lin)

Abstract

Graphene oxide (GO) membranes with tunable interlayer spacings are of interest for dye removal from salty textile wastewater, and the membranes are often reduced to improve their stability, which inevitably lowers water permeance. Herein, we demonstrate that reduced GO (rGO) membranes can be facilely modified using peracetic acid (PAA) in situ to dramatically enhance water permeance while retaining dye rejection. Specifically, PAA-modified membranes (PrGO) are synthesized by vacuum-filtering hydrazine-reduced rGO nanosheets onto Nylon substrate and then exposing them to PAA solutions. The effects of the rGO layer thickness, PAA content, and PAA exposure time on the membrane chemistry, nanostructures, and salt/dye separation properties are thoroughly examined. For example, the PAA oxidation of a 100 nm-thick rGO membrane for 10 min increases water permeance by 180%, from 35 to 93 liter m^{-2} h^{-1} bar^{-1}, and decreases Na_2SO_4 rejection from 10% to 3.3% while retaining the rejection of Congo red at ≈99.7%. The PrGO membranes exhibit stable water permeance and > 99% dye rejection in multi-cycle tests in a crossflow system, surpassing state-of-the-art GO membranes and showcasing their potential for practical applications.

Keywords: Reduced graphene oxide membrane; Peracetic acid; In situ oxidation; Dye desalination

1. Introduction

Textile industries release significant quantities of wastewater containing various dyes and salts (such as NaCl or Na_2SO_4) that are used to improve dyeing efficiency [1, 2]. Membrane technology, with high energy efficiency, low cost, and excellent scalability, has attracted substantial interest in recovering water and salts and mitigating dye release into the environment [3-5]. Membranes should have high permeance for water and salts and great dye rejection. However, existing commercial membranes optimized for other applications are not suitable for treating textile wastewater. For example, polyamide-based nanofiltration (NF) membranes show high rejection of both Na_2SO_4 and dyes [6]; ultrafiltration (UF) membranes can achieve high water and salt permeance but have low dye rejection [7]. Ideal membranes should have pore sizes larger than hydrated ions (6 - 8 Å) to attain high water and salt permeance but smaller than dye aggregates (10 - 100 nm) in aqueous solutions to reject dyes [6, 8].

Two-dimensional (2D) graphene oxide (GO) nanosheets have emerged as an appealing platform for designing membranes with desirable size-sieving channels [9-11]. The interlayer spacing is governed by the π–π interactions between adjacent nanosheets [8, 10, 12], and importantly, it can be manipulated by rich functional groups on GO nanosheets (including hydroxyl, carboxy, and epoxy groups). As GO nanosheets are hydrophilic and can be dispersed in aqueous solutions, directly deposited GO layers can be easily peeled off from the substrate during underwater operation. To overcome their underwater instability, the GO sheets are often cross-linked using polyamines [4, 13-16] or reduced thermally [10, 13] to improve their hydrophobicity and stability in water [17, 18]. Particularly, GO nanosheets can be chemically reduced using hydrazine [19], hydriodic acid [20], and vitamin C [21]. Regardless of the methods used to improve GO stability, the interlayer spacing of nanosheets is often decreased [22], decreasing water and

63 salt permeance. There is a delicate balance between the degree of GO reduction and the associated
64 trade-off between water and salt permeance and dye rejection because the degree of reduction may
65 not be easily manipulated during the one-step modification [23]. On the other hand, reduced GO
66 (rGO) nanosheets can be reversibly oxidized to optimize various properties [23, 24], such as
67 thermoelectric properties [25].

68 Herein, we demonstrate a facile approach to modify rGO membranes in situ with a model
69 oxidant to fine-tune interlayer spacings and improve salt/dye separation properties (Fig. 1). The
70 oxidant used in this study, peracetic acid (PAA, CH_3COOOH), is an organic peroxide that has
71 been used for disinfecting municipal wastewater and food washing water [26, 27]. PAA can
72 hydrolyze to produce hydrogen peroxide (H_2O_2) and acetic acid [28, 29], and it can react with C=C
73 bonds in rGO to reform epoxy groups [30-32]. Specifically, rGO membranes were prepared by
74 vacuum filtration of hydrazine-reduced GO nanosheets onto Nylon support and then treated with
75 PAA (100 - 500 ppm) in situ at ≈23 ℃ for 10 min to form PrGO membranes with enhanced surface
76 negative charge and improved water and salt permeance while retaining great dye rejection. For
77 instance, exposure to 250 ppm PAA doubles water permeance while maintaining < 5% rejection
78 for NaCl and Na_2SO_4 and >99% rejection for various dyes, including Congo red (CR), direct red
79 80 (DR 80), and methyl blue (MB) with molecular weight ranging from 697 to 1373 g/mol. Overall,
80 the PrGO membranes exhibit excellent dye removal performance for continuous crossflow
81 operation, demonstrating their potential for practical applications.
82

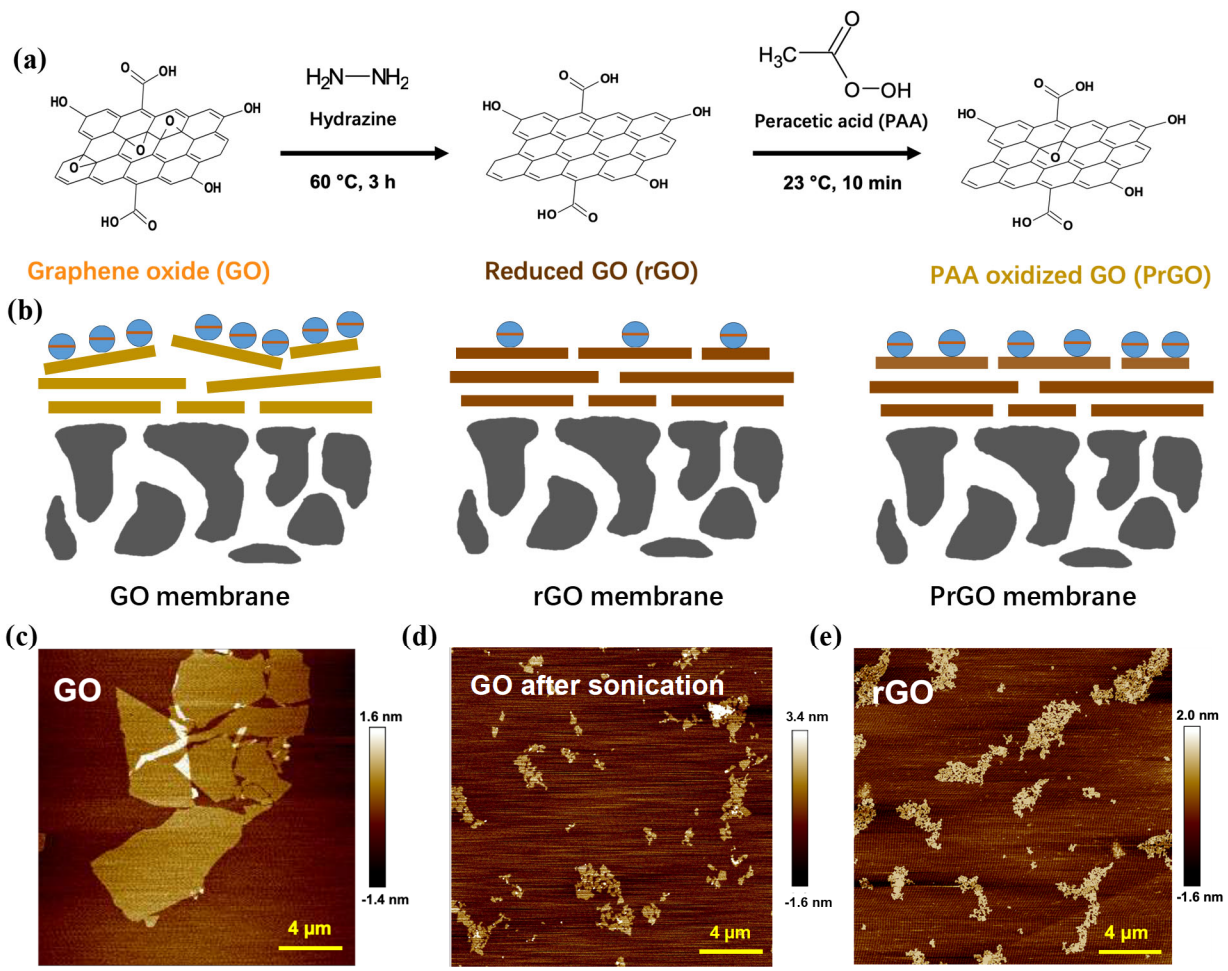

Fig. 1. Preparation of PrGOx/y membranes, where x and y represent the estimated rGO layer thickness (nm) and PAA concentration (ppm). (a) Chemical synthesis of PrGO, including hydrazine reduction of GO nanosheets and PAA oxidation. (b) Schematic of GO, rGO, and PrGO membranes. Atomic force microscope (AFM) images of (c) GO nanosheets, (d) GO nanosheets after ultra-sonication, and (e) rGO nanosheets.

2. Experimental

2.1. Materials

Natural graphite flakes (99%, 325 mesh), H_2O_2 (30 wt% in H_2O), H_2SO_4 (99%), $KMnO_4$ (≥ 99.0%), CR (697 Da), DR 80 (1373 Da), PAA (32% in acetic acid, containing 5.4% H_2O_2 in the equilibrium mixture), NaCl (≥ 99.0%), Na_2SO_4 (≥ 99.0%), and poly(ethylene glycol) (PEG, 2, 5, 10, 20, 35, and 100 kDa) were purchased from Sigma-Aldrich Corporation (St. Louis, MO). HCl (1.0 M) was obtained from Supelco (Bellefonte, PA). MB (800 Da) and isopropanol (IPA,

99%) were acquired from Fisher Scientific International (Pittsburgh, PA). Nylon support (a microfiltration (MF) membrane with a pore size of ~200 nm) was supplied by Cytiva (Marlborough, MA). The physical properties of the dyes are also recorded in Table S1.

2.2. Preparation of GO, rGO, and PrGO membranes

GO nanosheets were prepared from graphite flakes using a modified Hummer's method [4], and then they were reduced by hydrazine at 60 °C and pH = 10 after a probe ultrasonication [19, 33]. The obtained rGO nanosheets were fabricated into membranes (9.1 cm^2) on Nylon supports by vacuum filtration, and the amount of rGO deposited on the support can be used to estimate its theoretical thickness (x, nm) [19, 20]. The rGOx membranes were then exposed to PAA aqueous solutions (100 - 500 ppm) for 10 min before washing with deionized (DI) water (Fig. S1). The membranes were masked with impermeable plastic films to leave an active area of 2.9 cm^2 before being immersed in water prior to use.

2.3. Characterization of nanosheets and membranes

The chemical structures of rGO and PrGO membranes were characterized by a Vertex 70 FTIR spectrometer (Bruker, Billerica, MA) and a Raman spectrometer (Renishaw InVia, U.K.). The elemental composition of selective layers was analyzed using a PHI5000 VersaProbe II X-ray photoelectron spectroscopy (XPS, Physical Electronics Inc., Chanhassen, MN). Zeta potential was determined using a SurPASS 3 Surface Zeta Potential Analyzer (Anton Paar, Austria) with Ag/AgCl electrodes and a 0.01 M KCl electrolyte solution. The pH of the electrolyte solution was adjusted to 11 by adding a 0.05 M NaOH solution. Zeta potential measurements were taken in pH increments of ~0.5 from 11 to 3 through auto-titration with a 0.05 M HCl solution. The membrane surface was characterized for hydrophilicity using a Rame-Hart 190 contact angle goniometer (Succasunna, NJ).

Membrane surface roughness was obtained using an AFM (Bruker Dimension Icon with ScanAsyst, Bruker, Germany) in air tapping mode. Surface and cross-sectional images were taken by a focused ion beam (FIB) scanning electron microscope (SEM, Carl Zeiss, Germany). The *d*-spacing of selective layers was characterized using an X-ray diffractometer (XRD, Ultima IV diffractometer, Rigaku, Japan) with Cu Kα radiation (λ = 1.54 Å).

The sizes of dye aggregates in the aqueous solutions were determined using dynamic light scattering (DLS, Zetasizer Lab, Malvern, UK). Dye concentrations were determined by a Vernier UV−vis spectrophotometer (Vernier Software & Technology, Beaverton, OR).

Water permeance (A_W, liter m^{-2} h^{-1} bar^{-1} or LMH/bar) was determined using a dead-end filtration cell (HP4750, Sterlitech, Kent, WA) at a feed pressure of 1 bar. The A_W is calculated using Eq. 1 [34]:

$$A_W = \frac{J_W}{\Delta p} = \frac{1}{A_m \cdot \Delta p}\frac{dV}{dt} \quad (1)$$

where J_W is steady-state water flux (LMH), Δp is transmembrane pressure (bar), A_m is active membrane area (cm^2), and dV/dt is permeate flow rate (L h^{-1}).

The rejection (R, %) of dyes, salts, and PEGs can be calculated using Eq. 2:

$$R_i = \left(1 - \frac{C_{P,i}}{C_{F,i}}\right) \times 100\% \quad (2)$$

where C_F and C_P are the solute concentrations in the feed and permeate, respectively. The subscript i represents D for dyes, S for salts, and PEG for PEGs. The salt and PEG concentrations were determined using a conductivity meter and a total organic carbon (TOC) analyzer (Shimadzu, Japan), respectively.

The molecular weight cut-off (MWCO) of membranes was evaluated using 1 g/L PEG solutions, and it is defined as the molecular mass (M, Da) of PEG with 90% rejection. The

membrane pore size (a, nm) equals the Stokes radius of the PEG with 90% rejection and is given by [34, 35]:

$$a = 16.73 \times 10^{-3} M^{0.557} \quad (3)$$

The salt/dye separation factor (α) is calculated using Eq. 4:

$$\alpha = \frac{C_{P,S}/C_{F,S}}{C_{P,D}/C_{F,D}} = \frac{1-R_S}{1-R_D} \quad (4)$$

3. Results and discussion

3.1. Enhanced water permeance by PAA exposure

We wish to first highlight the unexpected increase in water permeance by PAA exposure. Fig. 2a,b shows the impact of PAA treatment conditions on membrane performance. Treatment by 100 ppm PAA does not substantially alter the water permeance or dye rejection for the membranes with 75 or 100 nm rGO layers; however, 250 ppm PAA treatment roughly doubles and triples the water permeance for these membranes, respectively. The PrGO100/250 exhibits water permeance of 105 ±13 LMH/bar and rejections of CR, DR 80, and MB greater than 99.5% (Fig. 2d). However, the PrGO75/250 membrane shows CR rejection of ~98% and DR 80 and MB rejection of < 96% (Fig. 2c) likely attributed to the formation of defects. Fig. S2 also confirms that increasing the rGO layer thickness decreases pure water permeance and increases dye and salt rejection, partially because of eliminated defects.

For rGO100, 100 or 250 ppm PAA treatment has no impact on dye rejection; >99.5% rejection is maintained for CR, DR 80, and MB (Fig. 2d). Further increasing PAA concentration to 500 ppm (PrGO100/500) leads to <90% rejection for all dyes because of defect formation as evidenced in the SEM image in Fig. 5e. Overall, the PrGO100/250 membrane exhibits the best performance, achieving both high water permeance and high dye rejection.

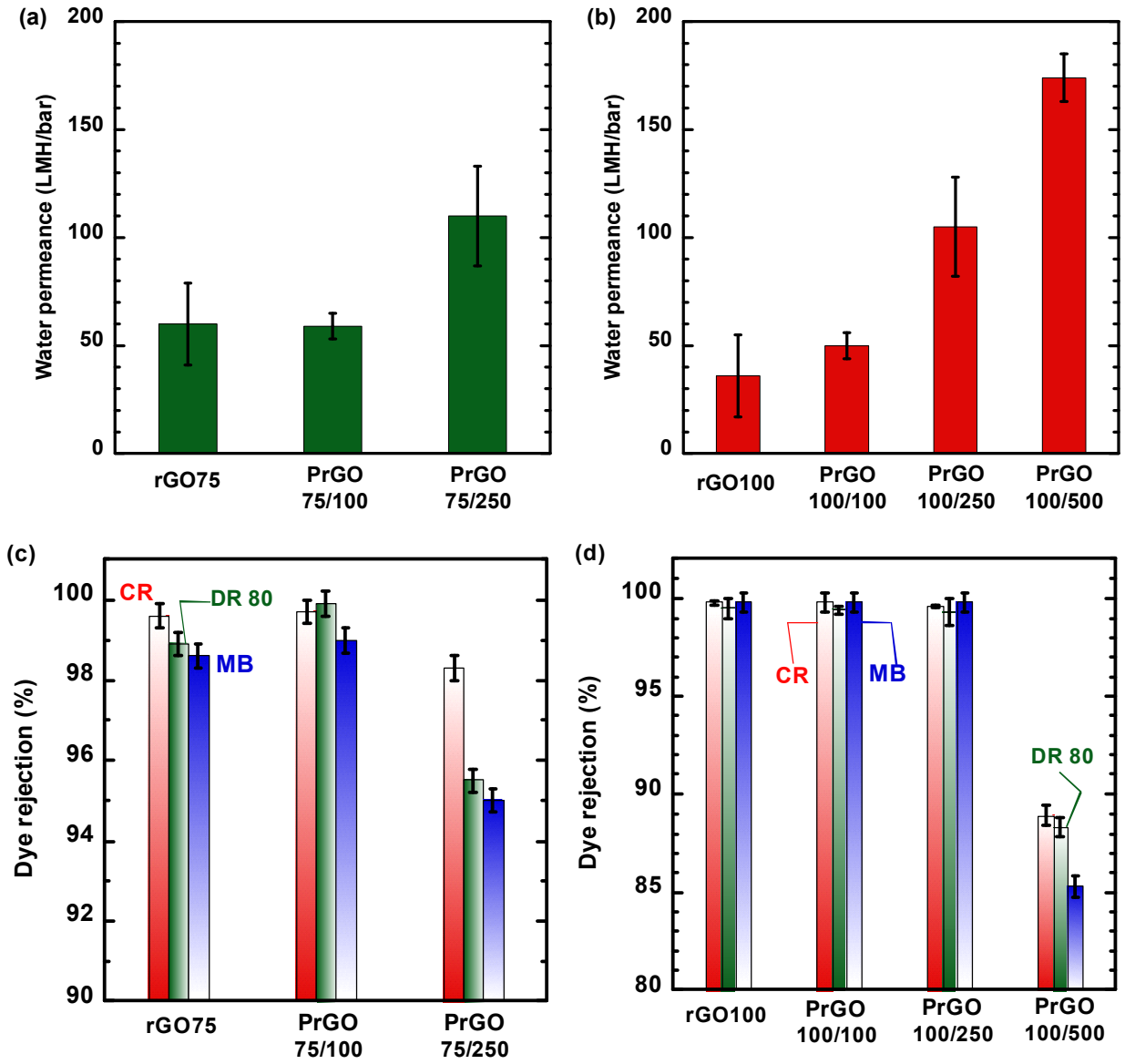

Fig. 2. Enhanced salt/dye desalination properties in PrGO membranes by PAA treatment. Pure water permeance for (a) rGO75 and (b) rGO100 membranes. CR, DR 80, and MB (0.2 g/L) rejection of (c) rGO75 and (d) rGO100 membranes. The error bar is the standard deviation for at least 3 membrane samples.

Fig. 3 compares the desalination performance of rGO100 and PrGO100/250 membranes as a function of the salt type and concentration. For both NaCl and Na_2SO_4 across concentrations ranging from 2 to 60 g/L [2], PrGO100/250 consistently exhibits lower salt rejection and higher water permeance than rGO100. At high salinity (60 g/L), PrGO100/250 also exhibits more

consistent water permeance (45 LMH/bar for Na_2SO_4 and 56 LMH/bar for NaCl) than rGO100 (13 LMH/bar for Na_2SO_4 and 35 LMH/bar for NaCl). For both membranes, increasing the NaCl and Na_2SO_4 content decreases their rejection and the associated water permeance, and the change is more significant for Na_2SO_4 than NaCl. For example, as the Na_2SO_4 content increases from 2 to 60 g/L, its rejection decreases from 14.4% to 1.2% for PrGO100/250 and from 20.9% to 7.4% for rGO100. Both membranes are negatively charged at pH = 7, and the high salinity decreases the Donnan potential and thus increases the SO_4^{2-} sorption, enhancing salt permeance [19, 36].

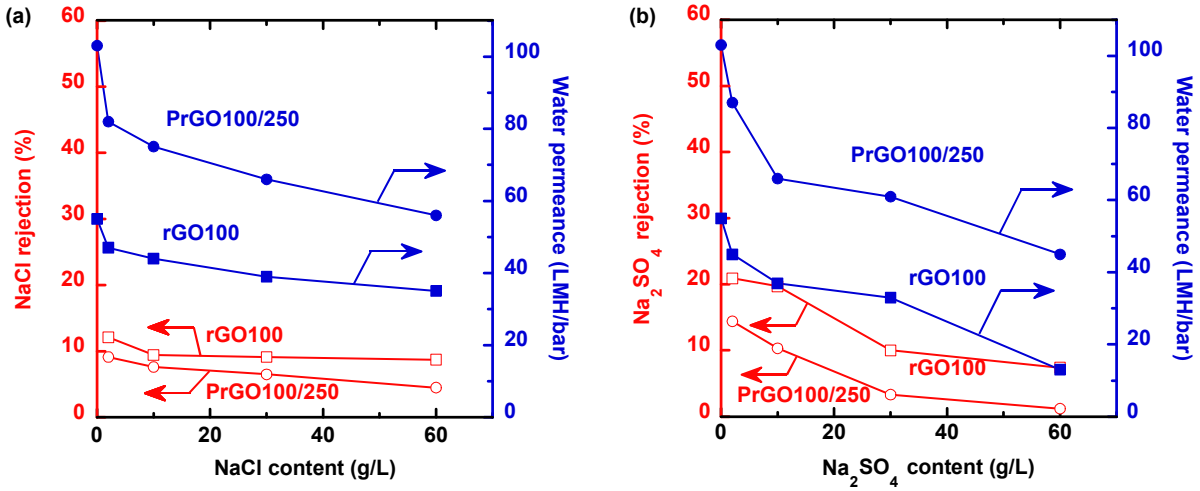

Fig. 3. Effect of the salt content on their rejection and water permeance in rGO100 and PrGO100/250 membranes for (a) NaCl and (b) Na_2SO_4.

Because PAA is an organic peroxide and its stock solution contains H_2O_2 as a stabilizer, we also synthesized an H_2O_2-treated rGO100 membrane (prepared by exposure to a 30% H_2O_2 solution at 23 °C for 10 min; HrGO100) and compared its performance with rGO100. A negligible difference in separation properties between HrGO100 and rGO100 membranes is observed (Fig. S3), suggesting an absence of reactions between the rGO and H_2O_2. Therefore, the difference between rGO and PrGO is caused by the direct reaction between the rGO and PAA.

3.2. Stability and dye desalination performance of PrGO membranes

The PrGO100/250 membrane, exhibiting both high water/salt permeance and high dye rejection, was challenged in a continuous four-cycle filtration test over 40 h in a crossflow system with 0.2 g/L MB in the feed. Fig. 4a shows that the membrane retains high water permeance and high MB rejection (> 99%), demonstrating its stability. Notably, when 0.2 g/L MB is used as the feed solution, the water permeance is 40% lower than its pure water permeance; using pure water feed after a cycle only slightly recovers water permeance, suggesting that dye adhesion within the PrGO layers is responsible for most of the water permeance loss. Nevertheless, the dye water permeance is very stable over the 40-hour test at ~ 45 LMH/bar.

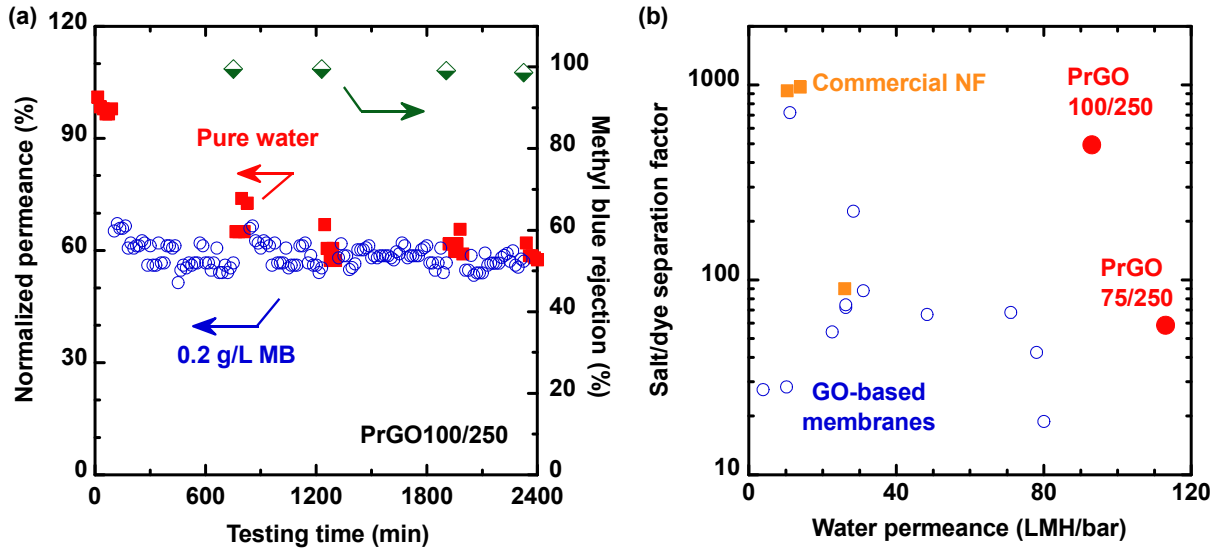

Fig. 4. Superior dye desalination in PrGO100/250 membranes. (a) Long-term stability test with 0.2 g/L MB for four cycles. (b) Comparison with state-of-the-art GO membranes [11, 37-45] and commercial NF membranes [46, 47]. Details are summarized in Table S2.

Fig. 4b compares the dye desalination performance, as indicated by the salt/dye separation factor and pure water permeance, between two PrGO membranes and the state-of-the-art GO-based membranes reported in the literature [11, 37-45] and commercial polyamide-based NF membranes [46, 47]. Compared with the GO membranes, our PrGO membranes exhibit much

higher water permeance and comparable or greater salt/dye separation factor. For example, PrGO100/250 exhibits a salt/dye separation factor roughly 50% lower than commercial Sepro NF6 membrane (which has the highest salt/dye separation factor among all membranes shown here), but its water permeance was 6.6 times greater.

3.3. Chemical and morphological structure of PrGO membranes

To explore the mechanism of PAA treatment for improving membrane performance, PrGO membranes were characterized by a suite of analytical tools and compared with the rGO membranes. Overall, PAA treatment does not create obvious changes in the apparent characteristics of the rGO membranes, such as thickness and morphology; its effects on the substantial improvement in membrane performance can be attributed to the fine-tuned surface chemistries of the rGO layer, including the O content and zeta potential.

The prepared GO nanosheets have a thickness of ~1 nm and lateral size of about 10 μm (Fig. 1c). Probe-ultrasonication and hydrazine reduction reduce the nanosheet sizes to < 4 μm (Fig. 1d,e). Unfortunately, the size of isolated PrGO nanosheets cannot be measured by AFM due to detachment from the mica substrate upon PAA treatment. Fig. S4a compares the UV-vis spectra of GO and rGO dispersion, and the peak shifts from 230 to 260 nm, validating the newly formed graphitic domains after reduction [19].

Fig. 5a,b displays that the deposition of rGO layers (≈100 nm thick) fully covers the pores of the Nylon support (~200 nm) and leads to wrinkle structures. Varying the PAA concentration between 100 and 250 ppm has no effect on the rGO surface morphology (Fig. 5c,d), but a further increase to 500 ppm generates small defects on the surface (Fig. 5e). Fig. 5f-j also compares the cross-sectional SEM images of Nylon, rGO100, and PrGO100. Both rGO and PrGO layers show

layered structures (which is typical for GO nanosheets), and their thicknesses are very close to the estimated thickness (≈100 nm), indicating that PAA treatment does not influence the selective layer thickness. Consistent with the results from SEM images, the AFM photos of the rGO/PrGO membranes show that PAA treatment does not have a major effect on local surface roughness (Fig. S4b-e).

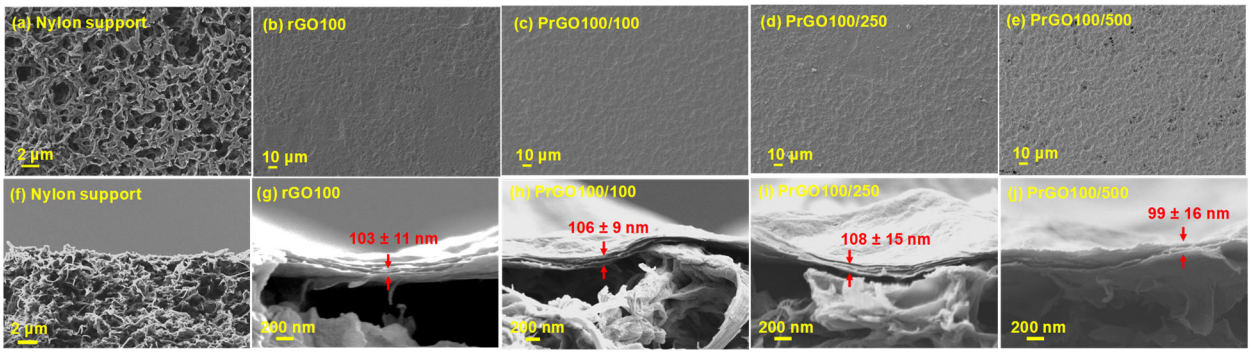

Fig. 5. Surface SEM images of (a) Nylon support, (b) rGO100 membrane, (c) PrGO100/100 membrane, (d) PrGO100/250 membrane, and (c) PrGO100/500 membrane. Cross-sectional SEM images of (f) Nylon support, (g) rGO100 membrane, (h) PrGO100/100 membrane, (i) PrGO100/250 membrane, and (j) PrGO100/500 membrane. The thickness uncertainty is the standard deviation for at least 3 membrane samples.

Raman spectroscopy analysis further shows that PAA exposure has a negligible effect on the crystalline structures of rGO (Fig. S5a): the rGO and PrGO membranes exhibit similar values of I_D/I_G, the ratio of peak intensity at 1350 and 1595 cm^{-1}, corresponding to the D band (disordered carbon structures) and G band (ordered graphitic structures), respectively [48]. Fig. S5b also shows that the PAA treatment does not significantly influence the water contact angle.

Fig. 6a compares the FTIR spectra of the GO100, rGO100, PrGO100/100, and PrGO100/250 membranes. All membranes exhibit the characteristic peaks of C-O stretching at 1350 and 1150 cm^{-1}; the signals were weaker for the rGO and PrGO membranes than GO100, consistent with the removal of epoxide groups by hydrazine reduction [49]. The subsequent PAA oxidation of rGO membrane does not significantly increase the C-O stretching peak, indicating

that the formation of new C-O moieties (e.g., epoxide or hydroxyl groups), if occurring, is relatively minor relative to the detection sensitivity of FTIR.

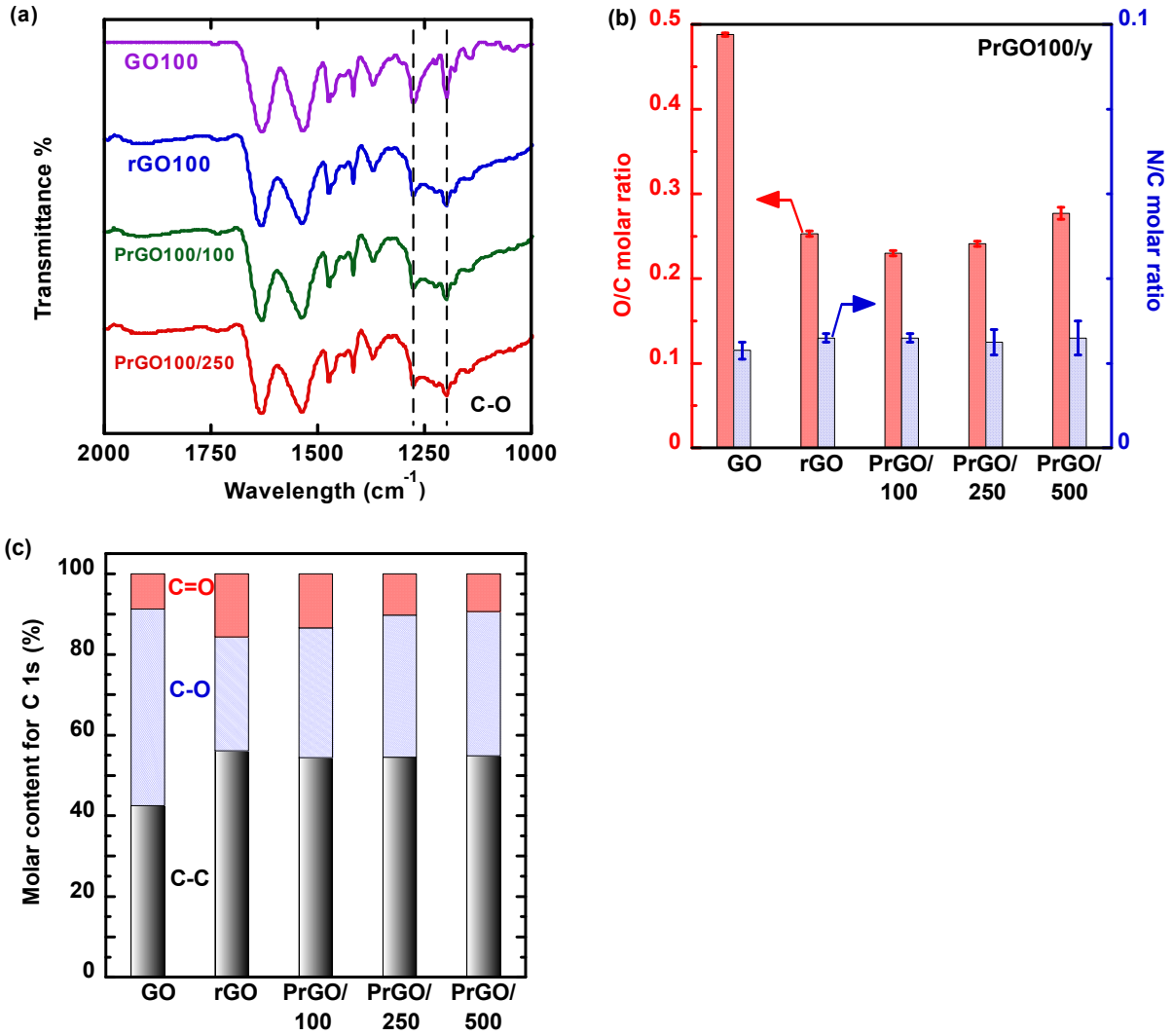

Fig. 6. Comparison of chemical structures of GO, rGO, and PrGO membranes. (a) FTIR spectra, (b) surface molar ratios of O/C and N/C, and (c) molar concentration of C-O, C=O, and C-C for C 1s from XPS. The uncertainty in b is the standard deviation for more than 3 membrane samples.

Compared with FTIR, XPS is more surface-sensitive and provides information for the top few nanometers of the materials. Fig. 6b and Table S3 compare the surface elemental composition of the GO, rGO, and PrGO membranes obtained from XPS analyses. The N/C ratios for GO and

rGO were similar [33, 50] and consistent with the proposed GO reduction pathways by hydrazine. As expected, the treatment with the PAA does not affect the N/C ratio either.

The hydrazine reduction significantly decreases the O/C ratio to 0.253±0.003, consistent with the removal of oxygen-containing functional groups as reported in the literature [50]. Surprisingly, the treatment of rGO with 100 ppm PAA further decreases the O/C molar ratio to 0.230±0.003. Exposure to higher concentrations of PAA solutions (250 and 500 ppm) gradually recovers and eventually increases the O/C ratios, such that the O/C ratio of PrGO100/500 was 0.277±0.007, exceeding that of rGO100, suggesting an epoxidation reaction [30]. To provide further mechanistic insight, attempts were made to deconvolute the C 1s peaks, as shown in Fig. S6 and Table S3. The C 1s peak is deconvoluted into three peaks [51] corresponding to C-C (284.6 eV), C−OH/C-O-C (286.5 eV), and C=O (287.8 eV) [52]; the O=C-O (289.0 eV) [53, 54] signal is not apparent. The mol% of C-O and C=O peaks can be used to infer the relative change of the oxygen-containing functional groups they each represent (Fig. 6c). As GO100 is reduced to rGO100, epoxide/hydroxyl groups are removed; with the overall decrease in O/C ratio, the increase in C=O mol% can be explained by the preferential removal of epoxide/hydroxyl groups over ketone groups by hydrazine. Between rGO100 and PrGO100/500, the latter has a higher O/C ratio but a lower C=O mol%, indicating that PAA treatment formed more epoxide/hydroxyl groups than ketone groups, consistent with the ability of PAA as an epoxidation agent [55, 56], the formation of epoxide/hydroxyl groups in 100 and 250 ppm PAA-treated rGO membranes is also supported by the data in Table S3.

Fig. 7a,b presents the XRD patterns of the rGO and PrGO membranes under dry and wet conditions (samples were prepared with 1 μm rGO/PrGO thickness for better resolution). Under dry conditions, the rGO100 membrane exhibits a peak at $2\theta = 15°$, corresponding to a *d*-spacing

of 0.59 nm, and the peaks for the 100 and 250 ppm PAA-treated PrGO membranes indicate very similar *d*-spacing (0.59 - 0.60 nm). Under wet conditions, a greater difference between rGO and PrGO is observed: the 15º peak for the rGO100 membrane shifts to < 5°, indicating an enhanced *d*-spacing of > 1.7 nm [19]. On the other hand, no corresponding peak is detected for PrGO100/100 and PrGO100/250, presumably because of even higher *d*-spacing values, which would be consistent with the greater water permeance of PrGO membranes [19].

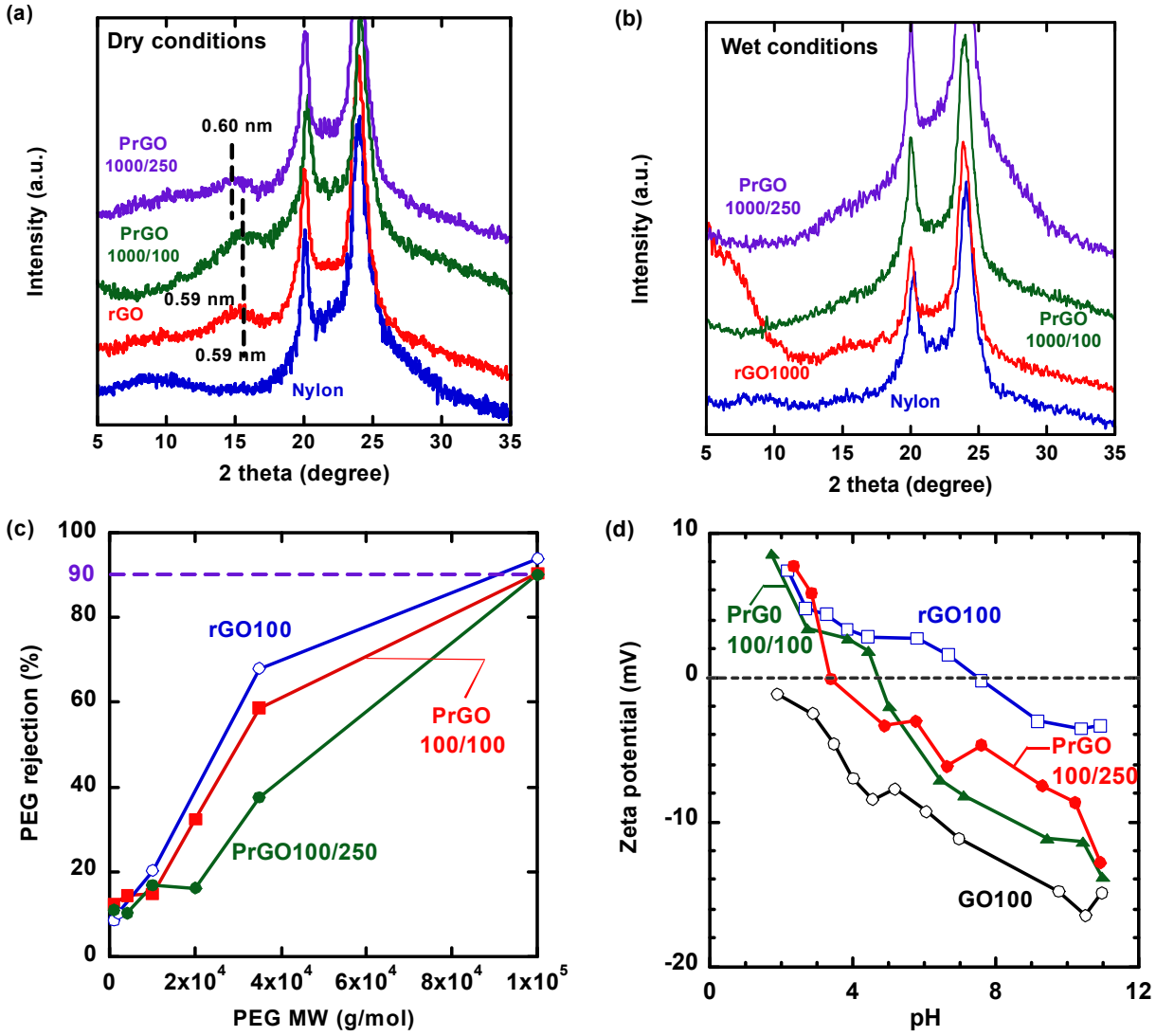

Fig. 7. Comparison of the XRD patterns of the Nylon support, rGO1000, PrGO1000/100, and PrGO1000/250 under (a) dry conditions and (b) wet conditions. (c) MWCO for the rGO100, PrGO100/100, and PrGO100/250 membranes. (d) Surface zeta potential for the membranes.

Fig. 7c shows the MWCO of the rGO100 and PrGO100 membranes determined using the PEGs (2 - 100 kDa). Both PrGO100/100 and PrGO100/250 membranes exhibit an MWCO of ≈99 kDa (corresponding to a nominal pore radius of 10 nm estimated using Eq. 3), similar to rGO100 (with an MWCO of 90 kDa and a nominal pore radius of 9.0 nm). Interestingly, considering that the membranes have a nominal pore radius larger than the size of individual dye molecules (2.4 - 4.5 nm; Table S1), the high rejection of dyes can be attributed to the formation of dye aggregates (≥ 300 nm) in aqueous solutions at textile wastewater-relevant concentrations (0.2 g/L) and salinity [57]. Indeed, DLS results suggest that CR, DR 80, and MR show particle hydrometers of 490 ± 270, 390 ± 250, and 360 ± 150 nm, respectively.

The surface zeta potential of the rGO membranes exhibits significant change after PAA treatment (Fig. 7d). The GO100 membrane surface is negatively charged at all testing pH (3 - 11), attributable to the abundance of carboxylic acid (-COOH) and hydroxyl (-OH) groups [58-60]. The rGO100 has an isoelectric point (IEP, defined as the pH value where the zeta potential is 0) of 7.7, and the PAA treatment at 100 and 250 ppm decreases the IEP to 5.1 and 3.6, respectively. At typical textile wastewater pH (~7) [2], the zeta potential of rGO is 2 mV; PAA treatment reduces the zeta potential to -7 mV for PrGO100/100 and -5 mV for PrGO100/250, closer to that of the GO membrane (-11 mV), as illustrated in Fig. 1b. Overall, these results suggest that PAA treatment increases the electronegativity on the rGO surface, which may be attributed to the formation of hydroxyl/carboxylic acid groups and/or an increase in these functional groups at the edge sites [60, 61]. Organic peracids (e.g., PAA) are known to oxidize ketone/aldehyde to ester/carboxylic acid (i.e., the Baeyer−Villiger reaction) or oxidize aromatic ring to form benzoquinone [62, 63]. The defects in PrGO100/500's SEM image suggest that PAA treatment can interrupt the nanosheets

and thereby create more edge sites; it is reasonable to expect a similar phenomenon to occur in PrGO100/100 and PrGO100/250 membranes.

Overall, the characterization results show that the enhanced performance of PrGO membranes is attributed to the small changes from the PAA treatment of rGO membranes. PrGO membranes exhibit similar surface morphology and crystallinity as rGO membranes, but PrGO membrane has a lower zeta potential. The observations that FTIR does not detect a change in the C-O signal and that XPS suggests the formation of epoxide/hydroxyl group indicate that the PAA modification of rGO chemistries is limited to the top few layers of nanosheets on the membrane surface. Although PAA can react with aromatic compounds to form benzoquinones, evidence is not strong in forming ketone groups on the PrGO surface.

4. Conclusions and perspectives

We demonstrate that the degree of oxidation and reduction of GO nanosheets can be fine-tuned to design thin rGO membranes with high permeance and excellent salt/dye separation properties. GO nanosheets are reduced by hydrazine and then fabricated into rGO membranes, which are then oxidized using PAA at 23 °C for only 10 min, as validated by XPS. The PAA exposure remarkably increases water permeance, slightly decreases salt rejection, and retains great dye rejection, which can be ascribed to the enhanced negative charges on the surface. Importantly, exposure to PAA solution at 250 ppm or lower has a negligible effect on the rGO thickness or hydrophilicity, and the mild fabrication conditions make it easy to scale up membrane fabrication. PrGO100/250 shows water permeance of over 100 LMH/bar and CR rejection of 99.7% with Na_2SO_4/dye separation factor as high as 490, surpassing the state-of-the-art NF membranes and GO membranes reported in the literature.

We expect that in situ oxidation with PAA can be a versatile approach to improving other reduced or cross-linked GO membranes developed, as PAA facilely imparts oxygen-containing groups on the GO nanosheets and improves water permeance. The PAA exposure may also be seamlessly combined with periodic membrane cleaning for fouling control in GO/rGO membrane systems. This approach could be adopted to improve separation performance for other 2D materials-based membranes.

Declaration of competing interest

The authors declare no conflict of interest.

Acknowledgment

We gratefully acknowledge the financial support from the U.S. National Science Foundation (2230728) and the Department of Energy Office of Energy Efficiency and Renewable Energy (DE-EE0009500). Work at The University of Texas at Austin (A.E.Q. and B.D.F.) was supported as part of the Center for Materials for Water and Energy Systems (M-WET), an Energy Frontier Research Center funded by the U.S. Department of Energy, Office of Science, Basic Energy Sciences under Award #DE-SC0019272.

Appendix A. Supplementary data

Supplementary data to this article can be found online at

References

[1] K. Paździor, L. Bilińska, S. Ledakowicz. A review of the existing and emerging technologies in the combination of AOPs and biological processes in industrial textile wastewater treatment. Chem. Eng. J. 376 (2019) 120597, 10.1016/j.cej.2018.12.057.

[2] D. A. Yaseen, M. Scholz. Textile dye wastewater characteristics and constituents of synthetic effluents: a critical review. Int. J. Environ. Sci. Technol. 16 (2018) 1193-1226, 10.1007/s13762-018-2130-z.

[3] W. Zhang, H. Xu, F. Xie, X. Ma, B. Niu, M. Chen, H. Zhang, Y. Zhang, D. Long. General synthesis of ultrafine metal oxide/reduced graphene oxide nanocomposites for ultrahigh-flux nanofiltration membrane. Nat. Commun. 13 (2022) 471, 10.1038/s41467-022-28180-4.

[4] X. Chen, E. Deng, X. Lin, A. M. Tandel, D. Rub, L. Zhu, L. Huang, H. Lin. Engineering hierarchical nanochannels in graphene oxide membranes by etching and polydopamine intercalation for highly efficient dye recovery. Chem. Eng. J. 433 (2022) 133593, 10.1016/j.cej.2021.133593.

[5] N. Li, T. Lou, W. Wang, M. Li, L. Jing, Z. Yang, R. Chang, J. Li, H. Geng. MXene-PANI/PES composite ultrafiltration membranes with conductive properties for anti-fouling and dye removal. J. Membr. Sci. 668 (2023) 121271, 10.1016/j.memsci.2022.121271.

[6] Y. Feng, X. Meng, Z. Zhang, L. Zhang. Dye retention and desalination behavior of MoS_2 doped high-flux β-CD/TDI polyurethane nanofiltration membrane. J. Membr. Sci. 656 (2022) 120643, 10.1016/j.memsci.2022.120643.

[7] Y. Wu, C. Fu, Q. Huang, P. Zhang, P. Cui, J. Ran, J. Yang, T. Xu. 2D Heterostructured Nanofluidic Channels for Enhanced Desalination Performance of Graphene Oxide Membranes. ACS Nano. 15 (2021) 7586-7595, 10.1021/acsnano.1c01105.

[8] A. R. Esfahani, C. Ma, U. A. Flewellen, S. Nair, T. A. L. Harris. Scalable aqueous-phase fabrication of reduced graphene oxide nanofiltration membranes by an integrated roll-to-roll (R2R) process. J. Membr. Sci. 678 (2023) 121669, 10.1016/j.memsci.2023.121669.

[9] X. Yan, S. Cheng, C. Ma, J. Li, G. Wang, C. Yang. D-spacing controllable GO membrane intercalated by sodium tetraborate pentahydrate for dye contamination wastewater treatment. J. Hazard. Mater. 422 (2022) 126939, 10.1016/j.jhazmat.2021.126939.

[10] Y. Li, W. Zhao, M. Weyland, S. Yuan, Y. Xia, H. Liu, J. Yang, C. Easton, C. Selomulya, X. Zhang. Thermally Reduced Nanoporous Graphene Oxide Membrane for Desalination. Environ. Sci. Technol. 53 (2019) 8314-8323, 10.1021/acs.est.9b01914.

[11] X. Zhang, H. Li, J. Wang, D. Peng, J. Liu, Y. Zhang. In-situ grown covalent organic framework nanosheets on graphene for membrane-based dye/salt separation. J. Membr. Sci. 581 (2019) 321-330, 10.1016/j.memsci.2019.03.070.

[12] H. Ma, X. Chen, S. Mohammed, Y. Hu, J. Lu, G. P. Simon, H. Hou, H. Wang. A thermally reduced graphene oxide membrane interlayered with an in situ synthesized nanospacer for water desalination. J. Mater. Chem. A. 8 (2020) 25951-25958, 10.1039/D0TA05790H.

[13] L. Cheng, K. Guan, G. Liu, W. Jin. Cysteamine-crosslinked graphene oxide membrane with enhanced hydrogen separation property. J. Membr. Sci. 595 (2020) 117568, 10.1016/j.memsci.2019.117568.

[14] F. Kong, Q. Liu, L. Dong, T. Zhang, Y. Wei, J. Chen, Y. Wang, C. Guo. Rejection of pharmaceuticals by graphene oxide membranes: Role of crosslinker and rejection mechanism. J. Membr. Sci. 612 (2020) 118338, 10.1016/j.memsci.2020.118338.

[15] M. Kumar, N. Sreedhar, N. Thomas, M. Mavukkandy, R. A. Ismail, T. M. Aminabhavi, H. A. Arafat. Polydopamine-coated graphene oxide nanosheets embedded in sulfonated poly(ether sulfone) hybrid UF membranes with superior antifouling properties for water treatment. Chem. Eng. J. 433 (2022) 133526, 10.1016/j.cej.2021.133526.
[16] Y. Liu, M. Zhu, M. Chen, L. Ma, B. Yang, L. Li, W. Tu. A polydopamine-modified reduced graphene oxide (RGO)/MOFs nanocomposite with fast rejection capacity for organic dye. Chem. Eng. J. 359 (2019) 47-57, 10.1016/j.cej.2018.11.105.
[17] J. Kang, Y. Choi, J. P. Kim, J. Kim, J. Kim, O. Kwon, D. I. Kim, D. Kim. Thermally-induced pore size tuning of multilayer nanoporous graphene for organic solvent nanofiltration. J. Membr. Sci. 637 (2021) 119620, 10.1016/j.memsci.2021.119620.
[18] J. Li, M. Hu, H. Pei, X. Ma, F. Yan, D. S. Dlamini, Z. Cui, B. He, J. Li, H. Matsuyama. Improved water permeability and structural stability in a polysulfone-grafted graphene oxide composite membrane used for dye separation. J. Membr. Sci. 595 (2020) 117547, 10.1016/j.memsci.2019.117547.
[19] L. Huang, S. Huang, S. R. Venna, H. Lin. Rightsizing Nanochannels in Reduced Graphene Oxide Membranes by Solvating for Dye Desalination. Environ. Sci. Technol. 52 (2018) 12649-12655, 10.1021/acs.est.8b03661.
[20] X. Chen, Z. Feng, J. Gohil, C. M. Stafford, N. Dai, L. Huang, H. Lin. Reduced Holey Graphene Oxide Membranes for Desalination with Improved Water Permeance. ACS Appl. Mater. Interfaces. 12 (2020) 1387-1394, 10.1021/acsami.9b19255.
[21] A. Jabbari, H. Ghanbari, R. Naghizadeh. Partial reduction of graphene oxide toward the facile fabrication of desalination membrane. Int. J. Environ. Sci. Technol. 20 (2023) 831-842, 10.1007/s13762-022-04592-z.
[22] E. L. Subtil, J. Gonçalves, H. G. Lemos, E. C. Venancio, J. C. Mierzwa, J. dos Santos de Souza, W. Alves, P. Le-Clech. Preparation and characterization of a new composite conductive polyethersulfone membrane using polyaniline (PANI) and reduced graphene oxide (rGO). Chem. Eng. J. 390 (2020) 124612, 10.1016/j.cej.2020.124612.
[23] Y. Hu, S. Song, A. Lopez-Valdivieso. Effects of oxidation on the defect of reduced graphene oxides in graphene preparation. J. Colloid Interface Sci. 450 (2015) 68-73, 10.1016/j.jcis.2015.02.059.
[24] O. Ö. Ekiz, M. Ürel, H. Güner, A. K. Mizrak, A. Dâna. Reversible Electrical Reduction and Oxidation of Graphene Oxide. ACS Nano. 5 (2011) 2475-2482, 10.1021/nn1014215.
[25] J. Choi, N. D. K. Tu, S.-S. Lee, H. Lee, J. S. Kim, H. Kim. Controlled oxidation level of reduced graphene oxides and its effect on thermoelectric properties. Macromol. Res. 22 (2014) 1104-1108, 10.1007/s13233-014-2160-4.
[26] C. Zoellner, A. Aguayo-Acosta, M. W. Siddiqui, J. E. Dávila-Aviña. Chapter 2 - Peracetic Acid in Disinfection of Fruits and Vegetables. In: Siddiqui MW, editor. Postharvest Disinfection of Fruits and Vegetables: Academic Press; 2018. p. 53-66.
[27] A. H. Hassaballah, J. Nyitrai, C. H. Hart, N. Dai, L. M. Sassoubre. A pilot-scale study of peracetic acid and ultraviolet light for wastewater disinfection. Environ. Sci. Water Res. Technol. 5 (2019) 1453-1463, 10.1039/c9ew00341j.
[28] M. Ghafari, T. M. Mohona, L. Su, H. Lin, D. L. Plata, B. Xiong, N. Dai. Effects of peracetic acid on aromatic polyamide nanofiltration membranes: a comparative study with chlorine. Environ. Sci. Water Res. Technol. 7 (2021) 306-320, 10.1039/d0ew01007c.
[29] A. H. Hassaballah, T. Bhatt, J. Nyitrai, N. Dai, L. Sassoubre. Inactivation of E. coli, Enterococcus spp., somatic coliphage, and Cryptosporidium parvum in wastewater by

peracetic acid (PAA), sodium hypochlorite, and combined PAA-ultraviolet disinfection. Environ. Sci. Water Res. Technol. 6 (2020) 197-209, 10.1039/c9ew00837c.
[30] S. Murahashi, T. Saito, H. Hanaoka, Y. Murakami, T. Naota, H. Kumobayashi, S. Akutagawa. Ruthenium-catalyzed oxidative transformation of alkenes to α-ketols with peracetic acid. Simple synthesis of cortisone acetate. J. Org. Chem. 58 (1993) 2929-2930, 10.1021/jo00063a002.
[31] R. D. Bach, C. Canepa, J. E. Winter, P. E. Blanchette. Mechanism of acid-catalyzed epoxidation of alkenes with peroxy acids. J. Org. Chem. 62 (1997) 5191-5197, 10.1021/jo950930e.
[32] S. Banfi, M. Cavazzini, G. Pozzi, S. V. Barkanova, O. L. Kaliya. Kinetic studies on the interactions of manganese–porphyrins with peracetic acid. Part 1. Epoxidation of alkenes and hydroxylation of aromatic rings. J. Chem. Soc., Perkin Trans. 4 (2000) 871-877, 10.1039/a905458h.
[33] X. Gao, J. Jang, S. Nagase. Hydrazine and thermal reduction of graphene oxide: Reaction mechanisms, product structures, and reaction design. J. Phys. Chem. C. 114 (2010) 832-842, 10.1021/jp909284g.
[34] E. Deng, X. Chen, D. Rub, H. Lin. Modeling and mitigating fouling of microfiltration membranes for microalgae dewatering. Sep. Purif. Technol. 315 (2023) 123707, 10.1016/j.seppur.2023.123707.
[35] S. Kasemset, L. Wang, Z. He, D. J. Miller, A. Kirschner, B. D. Freeman, M. M. Sharma. Influence of polydopamine deposition conditions on hydraulic permeability, sieving coefficients, pore size and pore size distribution for a polysulfone ultrafiltration membrane. J. Membr. Sci. 522 (2017) 100-115, 10.1016/j.memsci.2016.07.016.
[36] Z. H. Foo, D. Rehman, A. T. Bouma, S. Monsalvo, J. H. Lienhard. Lithium Concentration from Salt-Lake Brine by Donnan-Enhanced Nanofiltration. Environ. Sci. Technol. 57 (2023) 6320-6330, 10.1021/acs.est.2c08584.
[37] P. Zhang, J. Gong, G. Zeng, B. Song, S. Fang, M. Zhang, H. Liu, S. Huan, P. Peng, Q. Niu, D. Wang, J. Ye. Enhanced permeability of rGO/S-GO layered membranes with tunable inter-structure for effective rejection of salts and dyes. Sep. Purif. Technol. 220 (2019) 309-319, 10.1016/j.seppur.2019.03.041.
[38] P. Zhang, J. Gong, G. Zeng, B. Song, W. Cao, H. Liu, S. Huan, P. Peng. Novel “loose” GO/MoS_2 composites membranes with enhanced permeability for effective salts and dyes rejection at low pressure. J. Membr. Sci. 574 (2019) 112-123, 10.1016/j.memsci.2018.12.046.
[39] A. Ali, F. Rehman, M. Ali Khan, F. H. Memon, F. Soomro, M. Iqbal, J. Yang, K. H. Thebo. Functionalized Graphene Oxide-Based Lamellar Membranes with Tunable Nanochannels for Ionic and Molecular Separation. ACS Omega. 7 (2022) 32410-32417, 10.1021/acsomega.2c03907.
[40] L. Chen, J. Moon, X. Ma, L. Zhang, Q. Chen, L. Chen, R. Peng, P. Si, J. Feng, Y. Li, J. Lou, L. Ci. High performance graphene oxide nanofiltration membrane prepared by electrospraying for wastewater purification. Carbon. 130 (2018) 487-494, 10.1016/j.carbon.2018.01.062.
[41] M. Hu, B. Mi. Enabling Graphene Oxide Nanosheets as Water Separation Membranes. Environ. Sci. Technol. 47 (2013) 3715-3723, 10.1021/es400571g.
[42] L. Huang, Z. Li, Y. Luo, N. Zhang, W. Qi, E. Jiang, J. Bao, X. Zhang, W. Zheng, B. An, G. He. Low-pressure loose GO composite membrane intercalated by CNT for effective

dye/salt separation. Sep. Purif. Technol. 256 (2021) 117839, 10.1016/j.seppur.2020.117839.
[43] W. Zhang, M. Yin, C. Jin, Z. Liu, N. Wang, Q. An. Ice-crystal templating approach for tailoring mass transfer channels in graphene oxide membranes for high-performance dye/salt separation. Carbon. 183 (2021) 119-127, 10.1016/j.carbon.2021.06.077.
[44] J. Ma, X. Tang, Y. He, Y. Fan, J. Chen, H. Yu. Robust stable MoS_2/GO filtration membrane for effective removal of dyes and salts from water with enhanced permeability. Desalination. 480 (2020) 114328, 10.1016/j.desal.2020.114328.
[45] L. Dong, M. Li, S. Zhang, X. Si, Y. Bai, C. Zhang. NH_2-Fe_3O_4-regulated graphene oxide membranes with well-defined laminar nanochannels for desalination of dye solutions. Desalination. 476 (2020) 114227, 10.1016/j.desal.2019.114227.
[46] J. Lin, W. Ye, H. Zeng, H. Yang, J. Shen, S. Darvishmanesh, P. Luis, A. Sotto, B. Van der Bruggen. Fractionation of direct dyes and salts in aqueous solution using loose nanofiltration membranes. J. Membr. Sci. 477 (2015) 183-193, 10.1016/j.memsci.2014.12.008.
[47] J. Lin, W. Ye, M.-C. Baltaru, Y. P. Tang, N. J. Bernstein, P. Gao, S. Balta, M. Vlad, A. Volodin, A. Sotto, P. Luis, A. L. Zydney, B. Van der Bruggen. Tight ultrafiltration membranes for enhanced separation of dyes and Na_2SO_4 during textile wastewater treatment. J. Membr. Sci. 514 (2016) 217-228, 10.1016/j.memsci.2016.04.057.
[48] L. Cheng, Y. Guo, Q. Liu, G. Liu, R. Li, X. Chen, H. Zeng, G. Liu, W. Jin. Metal Confined in 2D Membranes for Molecular Recognition and Sieving towards Ethylene/Ethane Separation. Adv. Mater. 34 (2022) e2206349, 10.1002/adma.202206349.
[49] A. J. Page, C. P. Chou, B. Q. Pham, H. A. Witek, S. Irle, K. Morokuma. Quantum chemical investigation of epoxide and ether groups in graphene oxide and their vibrational spectra. Phys. Chem. Chem. Phys. 15 (2013) 3725-35, 10.1039/c3cp00094j.
[50] S. Park, J. An, J. R. Potts, A. Velamakanni, S. Murali, R. S. Ruoff. Hydrazine-reduction of graphite- and graphene oxide. Carbon. 49 (2011) 3019-3023, 10.1016/j.carbon.2011.02.071.
[51] H. Yu, P. Xu, D. W. Lee, X. Li. Porous-layered stack of functionalized AuNP–rGO (gold nanoparticles–reduced graphene oxide) nanosheets as a sensing material for the micro-gravimetric detection of chemical vapor. J. Mater. Chem. A. 1 (2013) 4444, 10.1039/c3ta01401k.
[52] S. Liu, G. Zhou, K. Guan, X. Chen, Z. Chu, G. Liu, W. Jin. Dehydration of C2–C4 alcohol/water mixtures via electrostatically enhanced graphene oxide laminar membranes. AlChE J. 67 (2021) aic17170, 10.1002/aic.17170.
[53] C. Dai, S. Li, Y. Duan, K. H. Leong, S. Liu, Y. Zhang, L. Zhou, Y. Tu. Mechanisms and product toxicity of activated carbon/peracetic acid for degradation of sulfamethoxazole: implications for groundwater remediation. Water Res. 216 (2022) 118347, 10.1016/j.watres.2022.118347.
[54] A. Aarva, V. L. Deringer, S. Sainio, T. Laurila, M. A. Caro. Understanding X-ray Spectroscopy of Carbonaceous Materials by Combining Experiments, Density Functional Theory, and Machine Learning. Part I: Fingerprint Spectra. Chem. Mater. 31 (2019) 9243-9255, 10.1021/acs.chemmater.9b02049.
[55] M. R. Janković, S. V. Sinadinović-Fišer, O. M. Govedarica. Kinetics of the Epoxidation of Castor Oil with Peracetic Acid Formed in Situ in the Presence of an Ion-Exchange Resin. Ind. Eng. Chem. Res. 53 (2014) 9357-9364, 10.1021/ie500876a.

[56] M. Musik, E. Milchert. Selective epoxidation of sesame oil with peracetic acid. J. Mol. Catal. 433 (2017) 170-174, 10.1016/j.mcat.2017.02.012.
[57] D. Talbot, J. Queiros Campos, B. L. Checa-Fernandez, J. A. Marins, C. Lomenech, C. Hurel, G. D. Godeau, M. Raboisson-Michel, G. Verger-Dubois, L. Obeid, P. Kuzhir, A. Bee. Adsorption of Organic Dyes on Magnetic Iron Oxide Nanoparticles. Part I: Mechanisms and Adsorption-Induced Nanoparticle Agglomeration. ACS Omega. 6 (2021) 19086-19098, 10.1021/acsomega.1c02401.
[58] Q. Xu, H. Xu, J. Chen, Y. Lv, C. Dong, T. S. Sreeprasad. Graphene and graphene oxide: advanced membranes for gas separation and water purification. Inorg. Chem. Front. 2 (2015) 417-424, 10.1039/c4qi00230j.
[59] S. Guo, S. Garaj, A. Bianco, C. Ménard-Moyon. Controlling covalent chemistry on graphene oxide. Nat. Rev. Phys. 4 (2022) 247-262, 10.1038/s42254-022-00422-w.
[60] M. Li, C. Liu, Y. Xie, H. Cao, H. Zhao, Y. Zhang. The evolution of surface charge on graphene oxide during the reduction and its application in electroanalysis. Carbon. 66 (2014) 302-311, 10.1016/j.carbon.2013.09.004.
[61] B. Konkena, S. Vasudevan. Understanding Aqueous Dispersibility of Graphene Oxide and Reduced Graphene Oxide through pKa Measurements. J. Phys. Chem. Lett. 3 (2012) 867-872, 10.1021/jz300236w.
[62] J. Kim, C.-H. Huang. Reactivity of Peracetic Acid with Organic Compounds: A Critical Review. ACS ES&T Water. 1 (2021) 15-33, 10.1021/acsestwater.0c00029.
[63] G. J. ten Brink, I. W. C. E. Arends, R. A. Sheldon. The Baeyer−Villiger Reaction: New Developments toward Greener Procedures. Chem. Rev. 104 (2004) 4105-4124, 10.1021/cr0300111.